JMEPEG (2010) 19:1043–1050
DOI: 10.1007/s11665-009-9577-5

1059-9495/$19.00

Effects of Minor Sr on As-Cast Microstructure and Mechanical Properties of ZA84 Magnesium Alloy

Mingbo Yang, Fusheng Pan, and Liang Cheng

(Submitted May 19, 2009; in revised form October 21, 2009)

The effects of minor Sr additions on the as-cast microstructure and mechanical properties of the ZA84 magnesium alloy were investigated. The results indicate that adding 0.05-0.15 wt.% Sr to the ZA84 alloy does not cause an obvious change in the morphology and distribution of the $Mg_{32}(Al,Zn)_{49}$ phase. However, the grains of the Sr-containing ZA84 alloys are effectively refined. Among the Sr-containing ZA84 alloys, the grains of the alloy added 0.10 wt.% Sr are relatively finer than other alloys. Furthermore, adding 0.05-0.15 wt.% Sr to the ZA84 alloy improves the tensile properties at room temperature and 150 °C but decreases the creep properties. Among the Sr-containing ZA84 alloys, the alloy added 0.10 wt.% Sr obtains the optimum tensile properties at room temperature and 150 °C.

Keywords magnesium alloy, metals and alloys, Sr, ZA84 magnesium alloy

1. Introduction

Magnesium alloys are the lightest structural alloys commercially available and have great potential for applications in automotive, aerospace, and other industries. At present, the widely used magnesium alloys are from the Mg-Al series alloys, such as AZ91 and AM60 alloys, but they are unsuitable for manufacturing parts operating at temperatures higher than 120 °C because of their poor creep resistance. Therefore, in recent years, improving the elevated temperature properties has become a critical issue for possible application of magnesium alloys in hot components. It has been reported that the ZA84 (Mg-8Zn-4Al) alloy is a potential elevated temperature magnesium alloy due to having moderate mechanical properties and good creep resistance, and satisfying the requirement of other corrosion and casting properties as compared with AZ91 alloy (Ref 1, 2). However, the castability and elevated temperature mechanical properties of the ZA84 alloy are not completely satisfying; further enhancement in the properties for the alloy needs to be considered by alloying and/or micro-alloying. Wang et al. (Ref 3) found that RE additions to the ZA84 alloy can modify the morphology, chemical compositions, and stability of the precipitates, thus leading to enhance the properties. However, based on the experimental results obtained by Wang et al. (Ref 3), RE addition to the ZA84 alloy results in an increase of solidification temperature range, which possibly decreases the casting fluidity. In addition, Balasubramani et al. (Ref 4) reported that Sb addition to the ZA84 alloy can refine the ternary $Mg_{32}(Al,Zn)_{49}$ phase besides forming Mg_3Sb_2 precipitates and having a little effect on the grain refinement. Both the room and elevated temperature strengths are found to increase in Sb added alloys with slight reduction in ductility.

Due to relatively high cost of RE addition and possible reduction of corrosion resistance resulting from individual addition of Sb (Ref 5), the applications of RE and Sb additions in the ZA84 alloy are not completely satisfying. Therefore, other micro-alloying elements such as Sr need to be considered in order to further improve the mechanical properties and castability of the ZA84 alloy. It has been reported that minor Sr can effectively refine the microstructures of the AZ (Mg-Al-Zn) and ZK (Mg-Zn-Zr) system alloys, thus leading to improve the mechanical properties (Ref 6-11). However, the investigation about the effect of Sr addition on the ZA (Mg-Zn-Al) system alloys is very scarce in the literature. Up to now, only Wan et al. (Ref 12) preliminarily investigated the effect of Sr addition on the microstructure and mechanical properties of the Mg-12Zn-4Al-0.23Mn (wt.%) alloy, and found that adding 0.2-0.8 wt.% Sr can improve the ultimate and yield strengths of the alloy. Due to the above-mentioned reasons, the present investigation aims to study the effects of minor Sr on the as-cast microstructure and mechanical properties of the ZA84 magnesium alloy.

2. Experimental

The Sr-containing ZA84 experimental alloys were prepared from pure Mg, Al, and Zn (>99.9 wt.%). The Sr was added in the form of Mg-10 wt.% Sr master alloy. The Mn was added in the form of Mg-4.38 wt.% Mn master alloy to decrease the iron content. The experimental alloys were melted in a crucible resistance furnace and protected by a flux addition. After being homogenized by mechanical stirring at 740 °C and mixed

Mingbo Yang, Materials Science & Engineering College, Chongqing University of Technology, Chongqing 400050, China and National Engineering Research Center for Magnesium Alloys, Chongqing University, Chongqing 400045, China; **Fusheng Pan**, National Engineering Research Center for Magnesium Alloys, Chongqing University, Chongqing 400045, China; and **Liang Cheng**, Materials Science & Engineering College, Chongqing University of Technology, Chongqing 400050, China. Contact e-mail: yangmingbo@cqut.edu.cn.

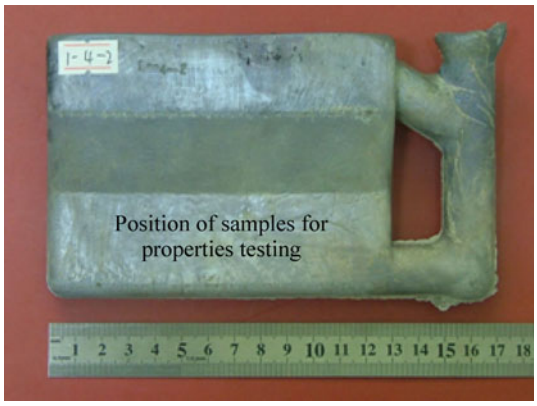

Fig. 1 Typical photograph of the cast sample

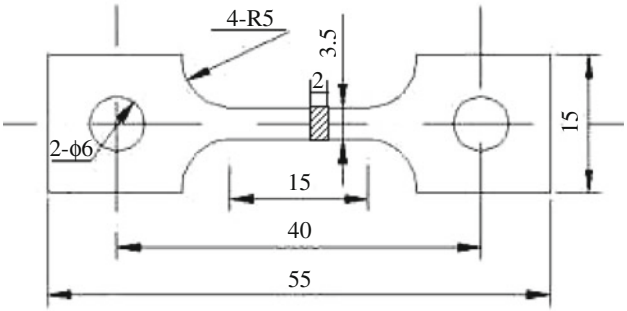

Fig. 2 Dimensions of the test samples (in mm)

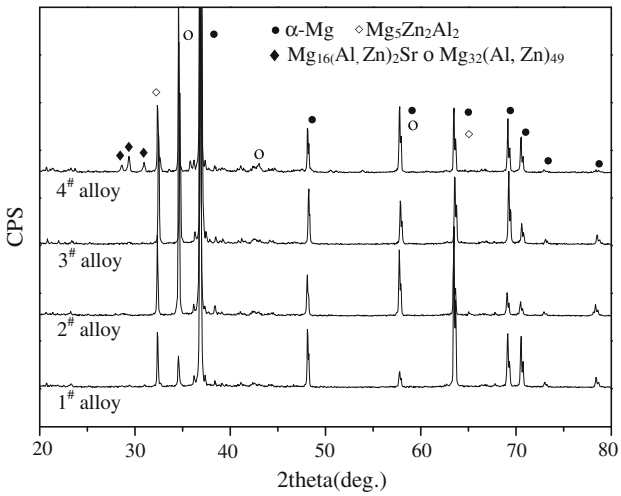

Fig. 3 XRD results of the as-cast alloys

Table 1 Actual compositions of the experimental alloys, wt.%

Nominal alloys	Zn	Al	Mn	Sr	Mg
1# (ZA84)	7.88	3.92	0.25	…	Bal.
2# (ZA84 + 0.05Sr)	7.88	3.90	0.24	0.032	Bal.
3# (ZA84 + 0.10Sr)	7.90	3.91	0.24	0.085	Bal.
4# (ZA84 + 0.15Sr)	7.89	3.92	0.25	0.129	Bal.

completely, the melt was held at 740 °C for 20 min and then poured into a permanent mould which was coated and preheated to 150 °C in order to obtain a casting as shown in Fig. 1. The non-standard tensile and creep specimens as shown in Fig. 2 were fabricated by cutting the samples in longitudinal direction of the casting. For comparison, the ZA84 alloy without adding Sr was also cast and machined into the same dimensions and tested under the same conditions as the above samples. Furthermore, the samples of the experimental alloys

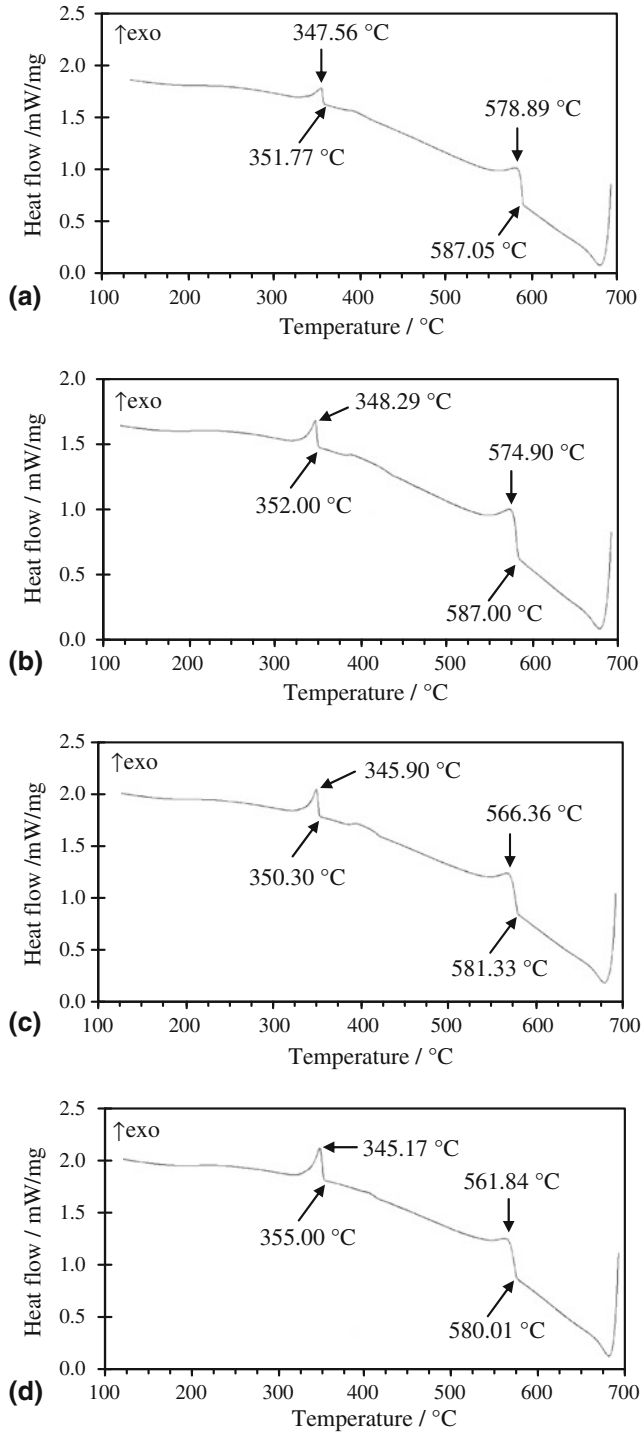

Fig. 4 DSC cooling curves of the as-cast alloys: (a) 1# alloy; (b) 2# alloy; (c) 3# alloy; and (d) 4# alloy

were subjected to an annealing treatment (340 °C/36 h, water cooled) in order to clearly reveal the grain boundaries. Table 1 lists the actual chemical compositions of the experimental alloys, which were analyzed by inductively coupled plasma spectroscopy.

In order to analyze the solidification behavior of the experimental alloys, the differential scanning calorimetry (DSC) was carried out by using a NETZSCH STA 449C system. Samples weighed around 30 mg were heated in a flowing argon atmosphere from 30 to 700 °C for 5 min before being cold down to 100 °C. The heating and cooling curves were recorded at a controlling speed of 15 °C/min.

The samples were etched in 8% nitric acid distilled water solution, and then examined by using an Olympus optical microscope and JEOL JSM-6460LV scanning electron microscope (SEM) with an operating voltage of 20 kV. The average grain size of the experimental alloys was measured by the standard linear intercept method using an Olympus stereomicroscope. The phases in the experimental alloys were analyzed by D/Max-1200X type x-ray diffraction (XRD) operated at 40 kV and 30 mA. The tensile tests were performed by CMT5105 type electromechanical universal testing machine of M/s MTS System (China) Co., Ltd. The tensile properties of the experimental alloys at room temperature and 150 °C were determined from a stress-strain curve. The ultimate tensile strength (UTS), 0.2% yield strength (YS), and elongation to failure (Elong.) were obtained based on the average of three tests. The constant-load tensile creep tests were performed by GWTA105 type high-temperature creep and relaxation testing machine of M/s MTS System (China) Co., Ltd. The total creep strain and minimum creep rate of the experimental alloys at 150 °C and 50 MPa for 100 h were measured from each elongation versus time curve.

3. Results and Discussion

3.1 Effect on As-Cast Microstructure

Figure 3 shows the XRD results of the as-cast experimental alloys. In general, in the ZA84 alloy, two main ternary phases are reported in the literature (Ref 13). One is identified as $Mg_{32}(Al,Zn)_{49}$ phase which has the cubic crystal structure (space group $Im\bar{3}$, a = 1.416 nm), and the other one is $Mg_5Zn_2Al_2$ phase having primitive orthorhombic structure (space group $Pbcm$, a = 0.8979 nm, b = 1.6988 nm, and c = 1.9340 nm). As shown in Fig. 3, the experimental alloys are mainly composed of α-Mg, $Mg_{32}(Al,Zn)_{49}$ and $Mg_5Zn_2Al_2$ phases. However, a new phase of $Mg_{16}(Al,Zn)_2Sr$, which has been reported in the literature (Ref 11), is identified in the ZA84 alloy added 0.15 wt.% Sr. Actually, the XRD results may be further confirmed by the DSC results of the experimental alloys. Figure 4 shows the DSC cooling curves of the as-cast experimental alloys. It is found from Fig. 4 that all the cooling curves are similar. There are two peaks in the cooling curves, corresponding to the α-Mg matrix melting and second phase transformation, respectively. Based on the Mg-Zn-Al phase diagram showing liquidus surfaces (Ref 14) and combined with the investigation of Zhang et al. (Ref 15), during the solidification of Mg-Zn-Al alloys the primary α-Mg phase first nucleates and grows until the temperature reaches about 343 °C where a binary eutectic reaction ($L_1 \rightarrow$ α-Mg + $Mg_5Zn_2Al_2$) first occurs and followed by a ternary quasi-peritectic reaction (L_2 + $Mg_5Zn_2Al_2 \rightarrow$ α-Mg + $Mg_{32}(Al,Zn)_{49}$). Finally, the binary eutectic reaction ($L_3 \rightarrow$ α-Mg + $Mg_{32}(Al,Zn)_{49}$) takes place. In this case, if the amount of the $Mg_5Zn_2Al_2$ phase was relatively large, they would not be used up in the ternary quasi-peritectic reaction. Accordingly, the final microstructure

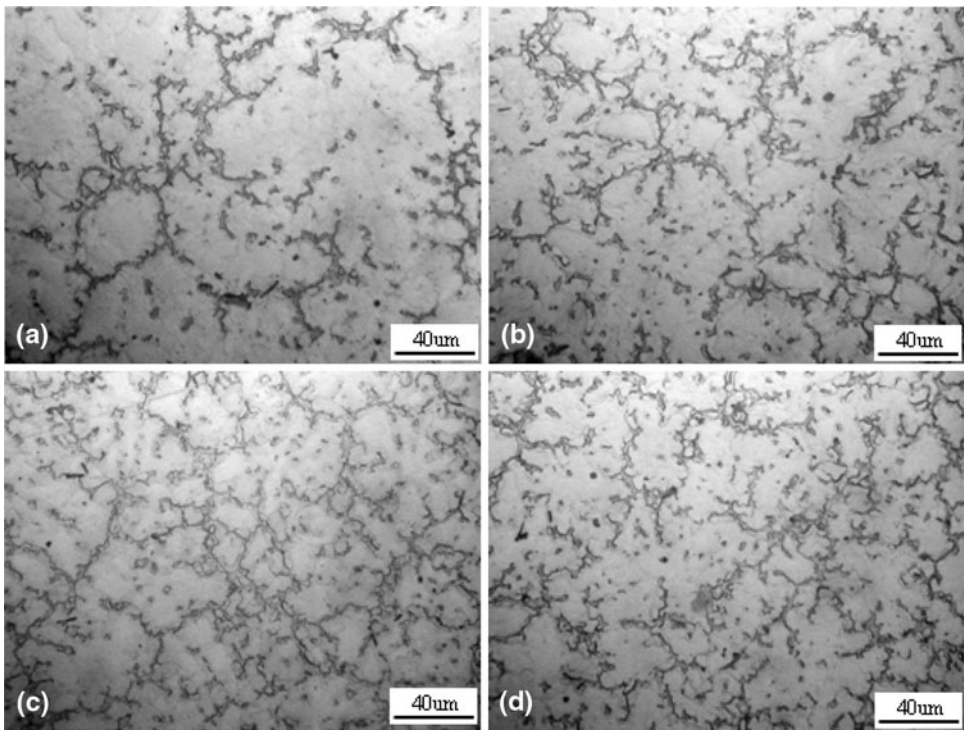

Fig. 5 Optical images of the as-cast alloys: (a) 1# alloy; (b) 2# alloy; (c) 3# alloy; and (d) 4# alloy

consists of α-Mg, $Mg_{32}(Al,Zn)_{49}$ and $Mg_5Zn_2Al_2$ phases as the studied ZA84 alloys in this work.

Figures 5 and 6 show the optical and SEM images of the as-cast experimental alloys, respectively. It is found from Fig. 5 and 6 that two types of precipitates having different morphologies are present in the as-cast microstructures of the experimental alloys. One has a continuous and/or quasi-continuous network, and the other has an isolated shape. According to the XRD and EDS results, the continuous and/or quasi-continuous precipitates are $Mg_{32}(Al,Zn)_{49}$ phase, the isolated phases are $Mg_5Zn_2Al_2$. Furthermore, it is observed from Fig. 5 and 6 that the morphology and distribution of the $Mg_{32}(Al,Zn)_{49}$ phases in the as-cast alloys seem to be similar, indicating that adding 0.05-0.15 wt.% Sr to the ZA84 alloy does not cause an obvious change in the morphology and distribution of the $Mg_{32}(Al,Zn)_{49}$ phase.

Figure 7 shows the optical images of the solutionized experimental alloys. It is found from Fig. 7 that the grains of the Sr-containing ZA84 alloys are finer than those of the ZA84 alloy without adding Sr. The average grain size of the 1#, 2#, 3#, and 4# alloys is 328, 216, 132, and 194 μm, respectively. The above results indicate that adding 0.05-0.15 wt.% Sr to the ZA84 alloy can effectively refine the grains of the alloy.

3.2 Effect on Mechanical Properties

The tensile properties, including ultimate tensile strength (UTS), 0.2% yield strength (YS), elongation (Elong.), and creep properties of the as-cast experimental alloys are listed in Table 2. Figures 8 and 9 show the low and high magnifications SEM images of tensile fractographs for the as-cast alloys tested at room temperature, respectively. Figure 10 shows the optical images of tensile longitudinal sections for the as-cast alloys tested at room temperature. As shown in Fig. 8 and 9, a number of cleavage planes and steps are present, and some minute lacerated ridges can also be observed in the localized areas of the tensile fracture surfaces, indicating that all the tensile fracture surfaces have the characteristic of cleavage fracture. In addition, it is observed from Fig. 10 that the tensile rupture of all the as-cast experimental alloys occurs along inter-granular boundary. The above results indicate that adding 0.05-0.15 wt.% Sr to the ZA84 alloy does not

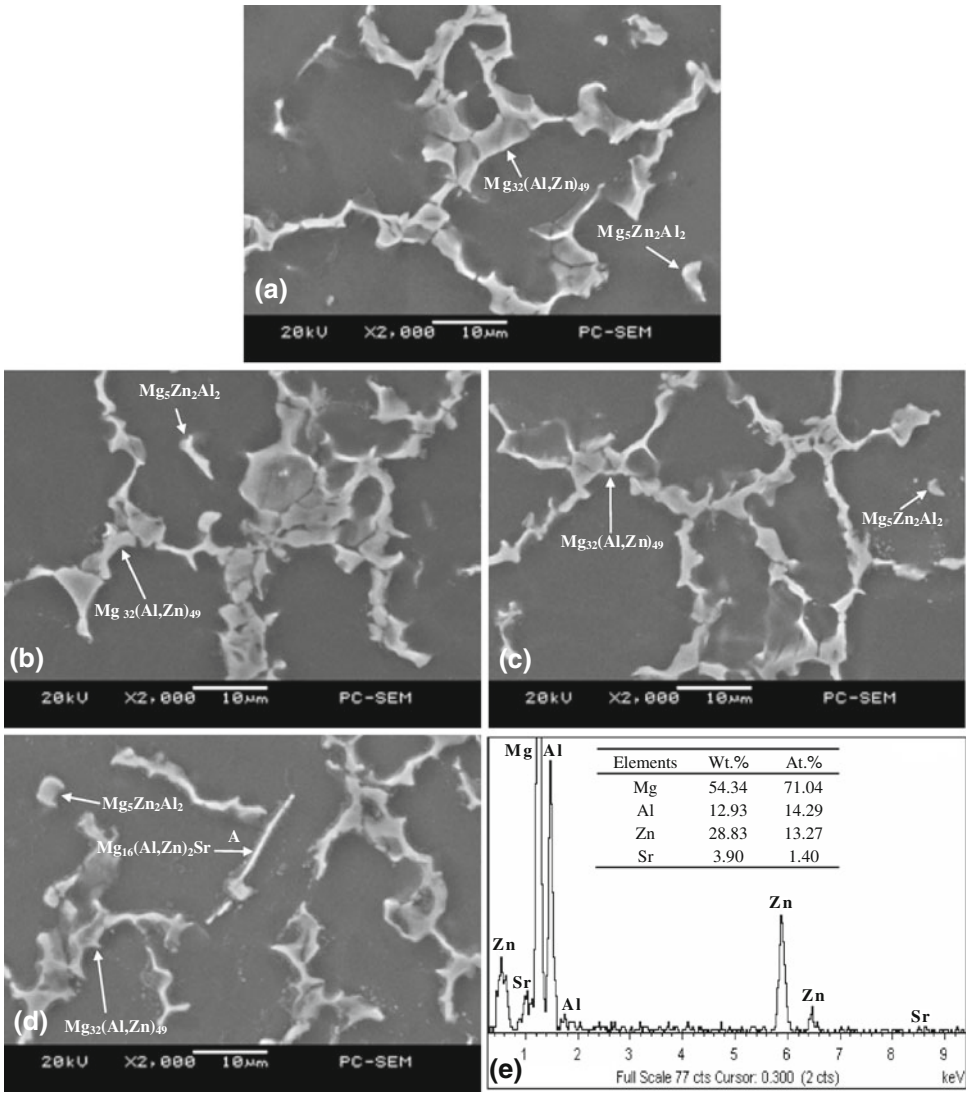

Fig. 6 SEM images of the as-cast alloys: (a) 1# alloy; (b) 2# alloy; (c) 3# alloy; (d) 4# alloy; and (e) EDS results of position A in (d)

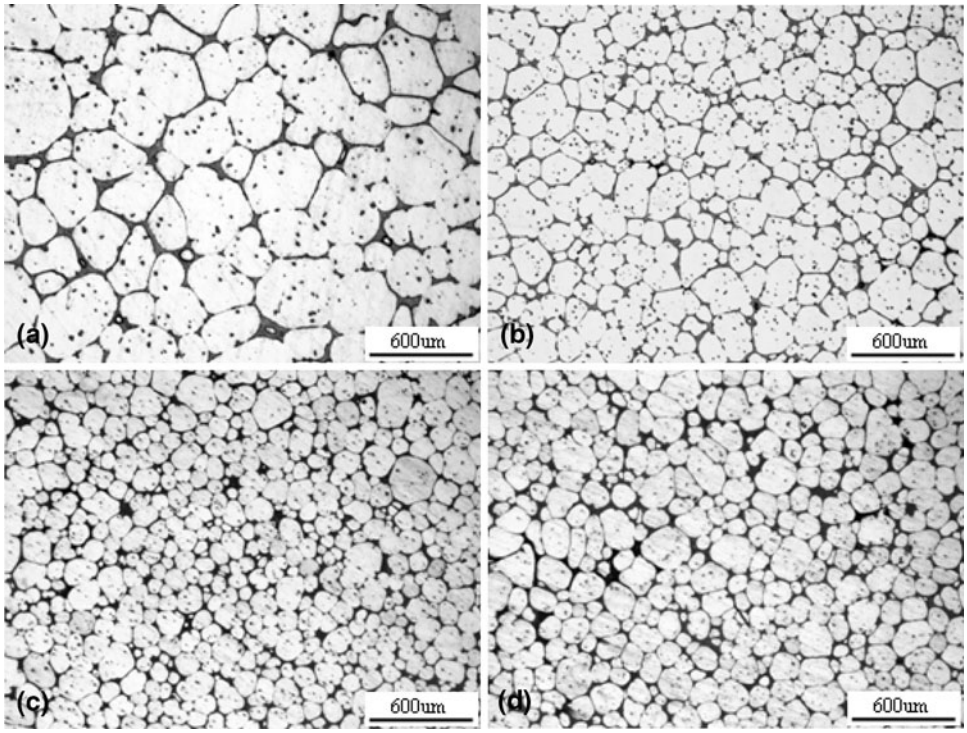

Fig. 7 Optical images of the solutionized alloys: (a) 1# alloy; (b) 2# alloy; (c) 3# alloy; and (d) 4# alloy

Table 2 Tensile and creep properties of the as-cast alloys

	Tensile properties						Creep properties	
	Room temperature			150 °C			150 °C and 50 MPa for 100 h	
Experimental alloys	UTS, MPa	YS, MPa	Elong., %	UTS, MPa	YS, MPa	Elong., %	Total creep strain, %	Minimum creep rate, $\times 10^{-8}$ s^{-1}
1# alloy	174 (3.8)	125 (2.3)	3.85 (0.19)	156 (2.8)	116 (4.1)	11.4 (1.1)	0.68	1.89
2# alloy	183 (3.1)	140 (2.5)	4.44 (0.22)	165 (3.5)	122 (2.1)	14.9 (2.0)	0.88	2.44
3# alloy	190 (2.9)	152 (3.3)	4.91 (0.26)	174 (2.7)	136 (3.5)	15.8 (1.8)	1.03	2.86
4# alloy	179 (3.2)	143 (2.8)	3.98 (0.18)	160 (3.0)	128 (2.2)	13.5 (1.6)	0.94	2.61

Note: the data in brackets indicates the standard error

significantly change the fracture mode of the alloy. However, it is observed from Table 2 that the 2-4# alloys exhibit relatively higher tensile properties at room temperature and 150 °C than the 1# alloy, indicating that adding 0.05-0.15 wt.% Sr to the ZA84 alloy can improve the tensile properties of the alloy. Furthermore, it is found from Table 2 that among the 2#, 3#, and 4# alloys, the 3# alloy exhibits relatively higher tensile properties than the 2# and 4# alloys. Obviously, the high tensile properties of the 3# alloy are consistent with its relatively small grain size. However, it is found from Table 2 that, although the grain size of the 4# alloy is relatively smaller than that of the 2# alloy, the tensile properties of the 4# alloy are relatively lower than those of the 2# alloy. This is possibly related to the formation of the needle-like $Mg_{16}(Al,Zn)_2Sr$ particle in the 4# alloy (Fig. 6d), which is possibly detrimental to the tensile properties (Ref 11). However, this needs further confirmation.

In addition, it is observed from Table 2 that the creep properties of the 2-4# alloys are lower than those of the 1# alloy, indicating that adding 0.05-0.15 wt.% Sr to the ZA84 alloy decreases the creep properties of the alloy. Furthermore, it is found from Table 2 that among the Sr-containing ZA84 alloys the creep properties of the alloy added 0.05 wt.% Sr are relatively high, followed by the alloys added 0.15 wt.% Sr and 0.10 wt.% Sr, respectively. The possible reason for the effect of minor Sr on the creep properties of the ZA84 alloy will be discussed in the following section.

3.3 Discussion

The above results indicate that adding 0.05-0.15 wt.% Sr to the ZA84 alloy can effectively refine the grains of the alloy, thus leading to increase the tensile properties. Since the mechanism for the grain refinement of the Sr-containing

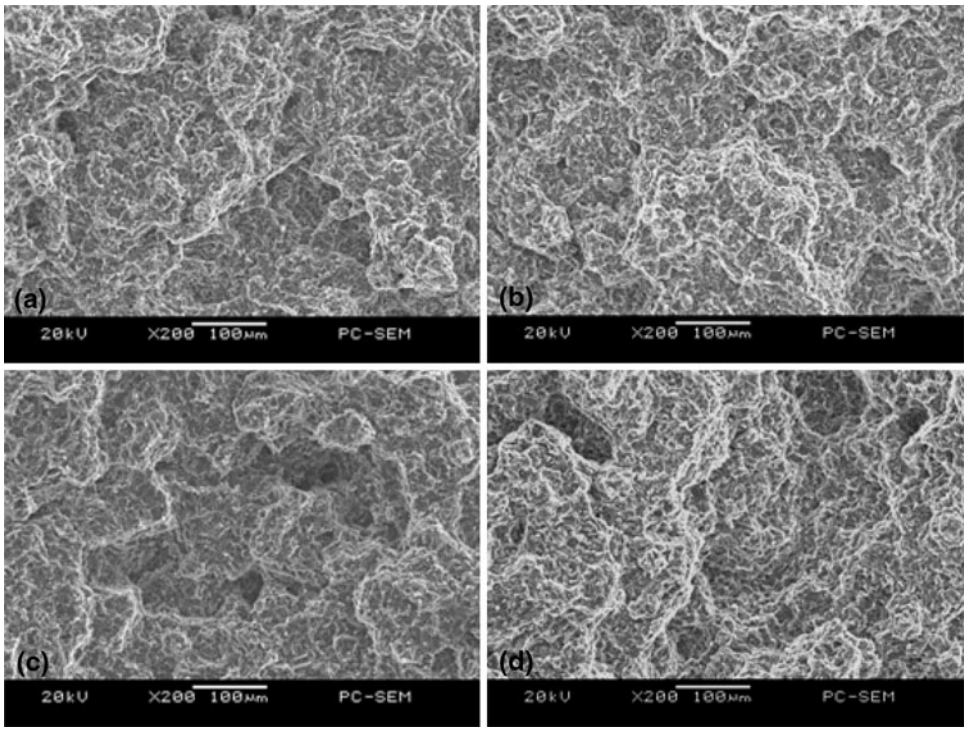

Fig. 8 Low-magnification SEM images of tensile fractographs for the as-cast alloys tested at room temperature: (a) 1# alloy; (b) 2# alloy; (c) 3# alloy; and (d) 4# alloy

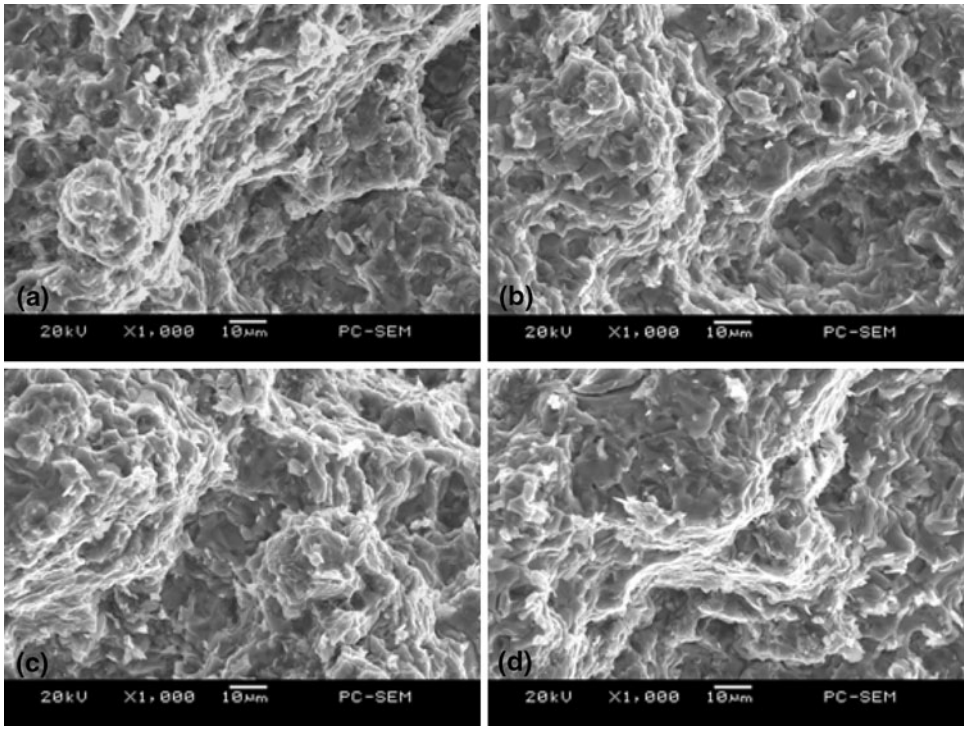

Fig. 9 High-magnification SEM images of tensile fractographs for the as-cast alloys tested at room temperature: (a) 1# alloy; (b) 2# alloy; (c) 3# alloy; and (d) 4# alloy

magnesium alloys has been described in detail in Ref 11, 16, the following discussions mainly focus on the difference in the grain refinement of the ZA84 alloys with different Sr amounts. In general, the grain refinement in industrial applications usually involves adding nucleants and/or solute elements into a melt before casting, and the effect of a solute element may be explained in terms of the growth restriction factor GRF (Eq 1) (Ref 16).

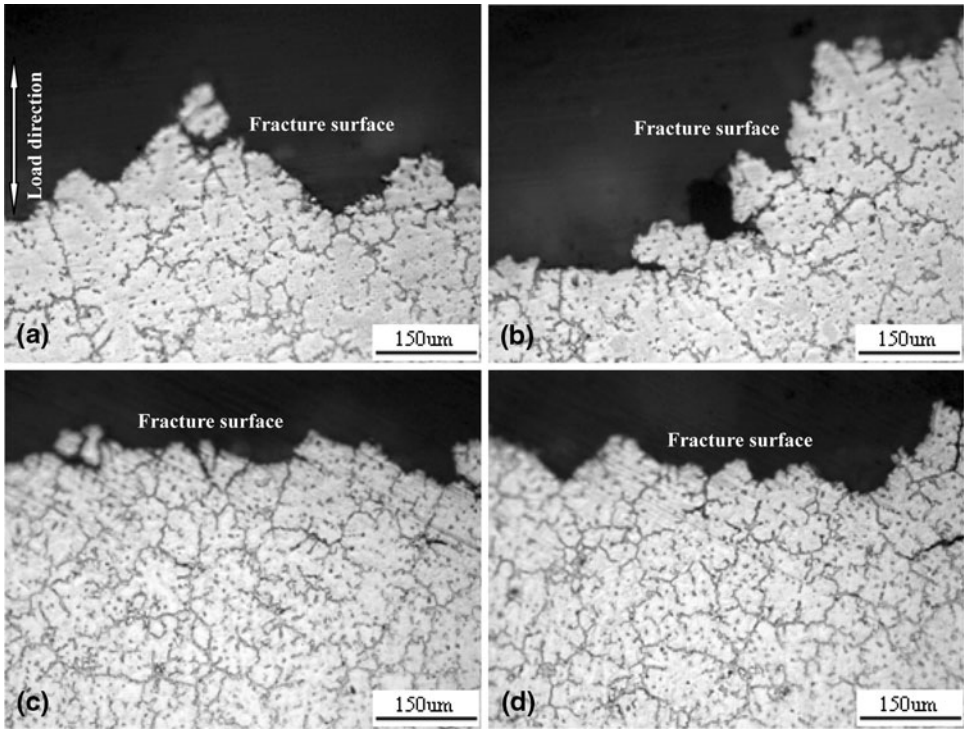

Fig. 10 Optical images of tensile longitudinal sections for the as-cast alloys tested at room temperature: (a) 1# alloy; (b) 2# alloy; (c) 3# alloy; and (d) 4# alloy

$$\mathrm{GRF} = \sum_i m_i c_{0i}(k_i - 1) \qquad \text{(Eq 1)}$$

where m_i is the slope of the liquidus line, c_{0i} is the initial concentration of element i, k_i is the partition coefficient. Under the experimental conditions of this work, i denotes Zn, Al, and Sr elements, respectively. According to Ref 11, $m_{Al} = -6.87$; $m_{Zn} = -6.04$; $m_{Sr} = -3.53$; $k_{Al} = 0.37$; $k_{Zn} = 0.12$; $k_{Sr} = 0.006$. The c_{0Al}, c_{0Zn}, and c_{0Sr} of the ZA84 alloys are listed in Table 1. Therefore, the GRF values of the ZA84 alloys added 0.05 wt.% Sr, 0.10 wt.% Sr, and 0.15 wt.% Sr are 58.87, 59.21, and 59.36 according to Eq 1, respectively. Based on the GRF mechanism, the bigger the GRF value, the higher is the refinement efficiency of a solute element. Obviously, the difference in the grain refinement of the ZA84 alloys added 0.05 wt.% Sr and 0.1 wt.% Sr can be easily explained by the GRF mechanism. However, the GRF mechanism is unsuitable for the difference in the grain refinement of the ZA84 alloys added 0.10 wt.% Sr and 0.15 wt.% Sr. The reason is possibly related to the formation of the $Mg_{16}(Al,Zn)_2Sr$ particle which reduces the effective grain growth restriction of Sr addition (Ref 11). However, this needs further confirmation.

In addition, the above results also indicate that adding 0.05-0.15 wt.% Sr to the ZA84 alloy decreases the creep properties of the alloy. Since the creep properties of magnesium alloys are mainly related to the structure stability at high temperatures, the effect of minor Sr on the creep properties of the ZA84 alloy is possibly related to the variation in microstructural features. Dispersion strengthening has been well known as one major strengthening mechanism for creep resistance of alloys (Ref 17). The second-phase particles can contribute to the creep resistance by obstructing dislocation movement in dislocation creep or inhibiting grain boundary migration and/or grain boundary sliding in diffusional creep. As shown in Fig. 5 and 6, the difference in the morphology and size of the second particles for the ZA84 alloys with and without adding Sr is not obvious. Obviously, the dispersion strengthening cannot explain the difference in the creep properties. The difference in the creep properties is possibly related to other mechanisms. It is generally accepted that the rate of dislocation creep tends to decrease with increasing grain size due to a lowered contribution of grain boundary sliding (Ref 17). Since the grain size of the Sr-containing ZA84 alloys is smaller than that of the ZA84 alloy without adding Sr, the grain size effect easily explains the difference in the creep properties of the ZA84 alloys with and without adding Sr. Similarly, the effect of Sr amount on the creep properties of the ZA84 alloy is possibly related to the difference of the grain size. In spite of the above analysis, the reason for the effect of minor Sr on the creep properties of the ZA84 alloy is not completely clear. For example, one question whether the $Mg_{16}(Al,Zn)_2Sr$ phase observed in the ZA84 alloy added 0.15 wt.% Sr has influence on the creep properties still remains. Therefore, further investigation still needs to be considered.

4. Conclusions

1. Adding 0.05-0.15 wt.% Sr to the ZA84 alloy can effectively refine the grains of the alloy. Among the Sr-containing ZA84 alloys, the alloy added 0.10 wt.% Sr exhibits relatively smaller grain size than other alloys.

2. Adding 0.05-0.15 wt.% Sr to the ZA84 alloy improves the tensile properties at room temperature and 150 °C but decreases the creep properties. Among the Sr-containing ZA84 alloys, the alloy added 0.10 wt.% Sr obtains the optimum tensile properties at room temperature and 150 °C.

Acknowledgments

The present work was supported by the National Natural Science Foundation of China (No. 50725413), the National Basic Research Development Program of China (973 Program) (No. 2007CB613704), and the Chongqing Education Commission of China (KJ090628).

References

1. J.H. Chen, Z.H. Chen, H.G. Yan, F.Q. Zhang, and K. Liao, Effects of Sn Addition on Microstructure and Mechanical Properties of Mg-Zn-Al Alloys, *J. Alloys Compd.*, 2008, **461**, p 209–215
2. M.B. Yang, F.S. Pan, R.J. Cheng, and J. Shen, Effects of Holding Temperature and Time on Semi-Solid Isothermal Heat-Treated Microstructure of ZA84 Magnesium Alloy, *Trans. Nonferrous Met. Soc. China*, 2008, **18**, p 566–572
3. Y.X. Wang, S.K. Guan, X.Q. Zeng, and W.J. Ding, Effects of RE on the Microstructure and Mechanical Properties of Mg-8Zn-4Al Magnesium Alloy, *Mater. Sci. Eng. A*, 2006, **416**, p 109–118
4. N. Balasubramani, A. Srinivasan, and U.T.S. Pillai, Effect of Sb Addition on the Microstructure and Mechanical Properties of ZA84 Magnesium Alloy, *J. Alloys Compd.*, 2008, **455**, p 168–173
5. A. Srinivasan, S. Ningshen, U.K. Mudali, U.T.S. Pillai, and B.C. Pai, Influence of Si and Sb Additions on the Corrosion Behavior of AZ91 Magnesium Alloy, *Intermetallics*, 2007, **15**, p 1511–1517
6. M.B. Yang, F.S. Pan, R.J. Cheng, and J. Shen, Comparison About Effects of Sb, Sn and Sr on As-Cast Microstructure and Mechanical Properties of AZ61-0.7Si Magnesium Alloy, *Mater. Sci. Eng. A*, 2008, **489**, p 413–418
7. M.B. Yang, F.S. Pan, R.J. Cheng, and A.T. Tang, Effect of Mg–10Sr Master Alloy on Grain Refinement of AZ31 Magnesium Alloy, *Mater. Sci. Eng. A*, 2008, **491**, p 440–445
8. M.B. Yang and F.S. Pan, Processing Effects on Grain Refinement of AZ31 Magnesium Alloy Treated with a Commercial Al-10Sr Master Alloy, *J. Mater. Eng. Perform.*, 2009, **18**, p 32–37
9. A. Srinivasan, U.T.S. Pillai, and J. Swaminathan, Observations of Microstructural Refinement in Mg-Al-Si Alloys Containing Strontium, *J. Mater. Sci.*, 2006, **41**, p 6087–6089
10. S.K. Guan, S.J. Zhu, L.G. Wang, Q. Yang, and W.B. Cao, Microstructures and Mechanical Properties of Double Hot-Extruded AZ80+*x*Sr Wrought Alloys, *Trans. Nonferrous Met. Soc. China*, 2007, **17**, p 1143–1151
11. X.Q. Zeng, Y.X. Wang, W.J. Ding, A.A. Luo, and A.K. Sachdev, Effect of Strontium on the Microstructure, Mechanical Properties, and Fracture Behavior of AZ31 Magnesium Alloy, *Metall. Mater. Trans. A*, 2006, **37**, p 1333–1341
12. X.F. Wan, Y.S. Sun, F. Xue, J. Bai, and W.J. Tao, Effects of Sr and Ca on the Microstructure and Properties of Mg-12Zn-4Al-0.3Mn Alloy, *Mater. Sci. Eng. A*, 2009, **508**, p 50–58
13. N. Balasubramani, U.T.S. Pillai, and B.C. Pai, Optimization of Heat Treatment Parameters in ZA84 Magnesium Alloy, *J. Alloys Compd.*, 2008, **457**, p 118–123
14. L. Bourgeois, B.C. Muddle, and J.F. Nie, The Crystal Structure of the Equilibrium Phase in Mg-Zn-Al Casting Alloys, *Acta Mater.*, 2001, **49**, p 2701–2711
15. Z. Zhang, R. Tremblay, and A. Coutune, Solidification Microstructure of ZA102, ZA104 and ZA106 Magnesium Alloys and Its Effect on Creep Deformation, *Can. Metall. Q*, 2000, **39**, p 503–512
16. Y.C. Lee, A.K. Dahle, and D.H. Stjohn, The Role of Solute in Grain Refinement of Magnesium, *Metall. Mater. Trans. A*, 2000, **31**, p 2895–2906
17. S.M. Zhu, B.L. Mordike, and J.F. Nie, Creep Properties of a Mg-Al-Ca Alloy Produced by Different Casting Technologies, *Mater. Sci. Eng. A*, 2008, **483–484**, p 583–586